Synthesis and controlled morphology of Ni@Ag core shell nanowires with excellent catalytic efficiency and recyclability

Shan Wang[1], Shaoyu Niu[1], Haosheng Li[1], Ka Kin Lam[2], Zongrong Wang[4,1], Piyi Du[4,1], Chi Wah Leung[4,2] and Shaoxing Qu[4,3]

1 State Key Lab of Silicon Materials, School of Materials Science and Engineering, Zhejiang University, Hangzhou, Zhejiang province, 310027, People's Republic of China

2 Department of Applied Physics, The Hong Kong Polytechnic University, Hung Hom, Hong Kong, People's Republic of China

3 Key Laboratory of Soft Machines and Smart Devices of Zhejiang Province, Zhejiang University, Hangzhou 310027, People's Republic of China

E-mail: zrw@zju.edu.cn, dupy@zju.edu.cn, apleung@polyu.edu.hk and squ@zju.edu.cn

Abstract

Ni@Ag core shell nanowires (NWs) were prepared by *in situ* chemical reduction of Ag^{+} around NiNWs as the inner core. Different Ni@Ag NWs with controllable morphologies were achieved through the layer-plus-island growth mode and this mechanism was confirmed by scanning electron microscopy, X-ray fluorescence, and X-ray photoelectron spectroscopy analyses. When used as a catalyst, the synthesized Ni@Ag NWs exhibited high reduction efficiency by showing a high reaction rate constant k of 0.408 s^{-1} in reducing 4-nitrophenol at room temperature. Besides, combining the magnetic property, including high saturation magnetization and low coercivity, the magnetic NiNW core contributes to excellent recyclability and long-term stability with only a 2.2% performance loss after 10 recycles by magnets. The Ni@Ag NWs proposed here show unprecedentedly high potential in applications requiring high efficiency and a recyclable catalyst.

Introduction

4-nitrophenol (4-NP) is a typical toxic substance that causes severe damage to both human health and the environment, and is still widely used in pesticides, insecticides, herbicides, etc. It can be absorbed through human skin and may irritate the eyes, skin, respiratory tract, and central nervous system of humans and animals. Therefore, how to effectively degrade this common harmful substance is an urgent problem to be solved and has attracted wide attention in recent years [1–10]. The reduction product of 4-NP is 4-aminophenol (4-AP), which is non-toxic and could be used as corrosion inhibitor, drying agent, and a precursor for manufacturing analgesic and antipyretic drugs [11, 12]. 4-NP has been reported to be reduced by sodium borohydride ($NaBH_4$) with the assistance of many traditional nanocatalysts [13], including silver [14], platinum [15], gold [16], etc. Additionally, due to the comparatively low cost, silver nanoparticles (AgNPs) have been widely used as catalysts in many chemical reactions [14, 17–21], especially in the reduction of 4-NP [19, 22, 23].

However, the complete separation and collection of these traditional nanocatalysts from polluted water is a critical problem, which limits the reusability and further makes the cost high. Many researchers have proposed combining AgNPs and magnetic materials to form composites, such as Fe, Co, Ni, and oxides, and then the composite could be easily separated from the medium by magnetic field [24–29]. Roy *et al* synthesized Ni core/Ag shell nanoparticles (Ni@AgNPs) by a simple chemical route and studied the effect of Ag coating on the magnetic properties of NiNPs [30]. Zhu and co-authors also reported nanocomposites with a AgNP shell on magnetic Fe_3O_4@C core as a catalyst for the reduction of 4-NP and methylene blue [29].

However, the main problem of the small-sized magnetic AgNPs when used as catalysts is the aggregation caused by their high surface energies, which can seriously decrease the catalytic

efficiency [31, 32]. In addition, the small size and weak magnetic interactions of ordinary NP catalysts make them difficult to collect by an external magnetic field. A large portion of catalysts were lost and caused great wastage [22, 33]. If a new kind of catalyst with high catalytic efficiency and stable recycling performance could be proposed, the problem of catalyst loss could be solved and the catalysts could be used for a greater number of cycles to reduce costs.

In this work, Ni@Ag core shell nanowires (NWs) were synthesized by *in situ* chemical reduction of Ag^{+} around NiNWs as the inner core and were used as catalysts to reduce 4-NP. Compared with traditional NP catalysts, the core shell NWs catalyst displays many unprecedented advantages. The Ag shell consisting of AgNPs could not only provide high catalytic activity on reduction of 4-NP, but also improve the anti-oxidation of Ni core, leading to higher efficiency and stability. Combining the magnetic property of a NiNW core, the excellent cycle performance of the Ni@Ag NWs catalyst could also be ensured.

Experimental section

Synthesis of Ni@Ag NWs

NiNWs were synthesized by a chemical reduction method under external magnetic field according to a previous work [34]. For the synthesis of Ni@Ag NWs, 1 mmol of NiNWs were dispersed in 50 ml of deionized water (0.02 mol l^{-1}) and a certain amount of polyvinylpyrrolidone was added into the solution as a surface modification agent to prevent the NiNWs from agglomerating. Then, the solution was sonicated for 10 min to make the NiNWs uniformly dispersed and was mixed with an equal volume of $AgNO_3$ solution with the concentrations of 0.01, 0.02, and 0.06 mol l^{-1}, respectively. The solution then became green then,

revealing the replacement of Ni by Ag. After that, 5 ml of hydrazine hydrate (85 wt%) was added dropwise and the solution turned beige, indicating the formation of NiAg composites.

Characterization

The X-ray diffraction (XRD) patterns of Ni@Ag NWs were characterized by a Philips X'Pert PRO diffractometer (Cu Kα, λ = 1.5406 Å) with an accelerating voltage of 40 kV and an applied current of 40 mA. X-ray fluorescence (XRF; EAGLE III) analysis was used to evaluate the mole ratio of [Ag]:[Ni] of Ni@Ag NWs. A scanning electron microscope (SEM; Hitachi S4800) and transmission electron microscope (TEM; TF 20) were used to analyze the morphologies. High-resolution TEM (HRTEM) and selected area electron diffraction (SAED) were used to verify the structure. Thermogravimetric analysis (TGA) was carried out on a dried sample in air at a heating rate of 5 °C min^{-1} on a NETZSCH TG209F3 instrument. X-ray photoelectron spectroscopy (XPS) measurement was conducted using the Escalab 250Xi spectrometer equipped with a Mg Kα X-ray source. The magnetic properties of the Ni@Ag NWs were analyzed by a MPMS-XL-5 superconducting quantum interference device.

Catalytic reduction of 4-NP

At first, 5 ml of freshly prepared 0.2 mol l^{-1} $NaBH_4$ solution was added into a 100 ml 0.1 mmol l^{-1} 4-NP solution as a reducing agent. The color of the solution turned from light yellow to deep yellow immediately. Then, 5 mg of Ni@Ag NWs catalyst were added and the yellow solution gradually faded as the reaction proceeded. At the same time, the reduction of 4-NP to 4-AP was monitored by recording the intensities of the absorption peaks of the reactant. About 3 ml of the mixture was filtered through a 0.22 μm membrane filter every 2 min and measured with ultraviolet–visible (UV–vis) absorption spectra in the range of 250–500 nm. The cycle

performance was investigated to evaluate the recyclability of the catalysts. After the reaction finished, the catalysts were magnetically separated by a magnet. After that the new solution was added and the reaction was repeated under the same conditions.

Results and discussion

Formation mechanism of Ni@Ag NWs

Two main reactions occurred during the synthesis of the Ni@Ag NWs, as shown in the schematic diagram in figure 1.

Firstly, a transmetallation reaction between an Ni atom and Ag^+ occurred during the mixing of the NiNW and $AgNO_3$ solution since the redox potential of transmetallation is +1.03 V > 0, which is an energetically favorable reaction. A few layers of Ni atoms on the NiNW core were consumed in the transmetallation reaction and were be replaced with Ag following equation (1). As a result, a thin layer of Ag was formed *in situ* on the surface of NiNWs.

$$\begin{aligned} &Ag^+ + e^- \rightarrow Ag^0 \quad E^\theta(Ag^+/Ag) = +0.80\ V \\ &Ni^{2+} + 2e^- \rightarrow Ni^0 \quad E^\theta(Ni^{2+}/Ni) = -0.23\ V \\ &Ni^0 + 2Ag^+ \rightarrow Ni^{2+} + 2Ag^0 \quad E^\theta(Ag^+/Ag \\ &\qquad -Ni^{2+}/Ni) = +1.03\ V \end{aligned} \tag{1}$$

Meanwhile, Ag^+ was directly reduced to Ag islands by hydrazine hydrate and gradually formed the Ag shell. The whole process of synthesizing Ni@Ag NWs was similar to the layer-plus-island (Stranski–Krastanov (S–K)) growth mode [35]. The Ag layer was reduced *in situ* by transmetallation reaction on the surface of the NiNW. After that, Ag^+ starts to be reduced by hydrazine hydrate and the resulting Ag atoms were deposited on the surface of the NiNWs to form Ag islands. As the reduction continued, the area of the Ag islands increased by the growth

of pre-existing small islands and the merging among these islands, which is known as Ostwald ripening [36]. A Ag shell were formed when these islands completed connecting with each other. The XRD patterns of Ni@Ag NWs with different mole ratios of Ag to Ni in the sources ([Ag]:[Ni]) are shown in figure 2. The peaks at $2\theta = 38.1°$, 44.3°, 64.4°, 77.5°, and 81.5° correspond to the (111), (200), (220), (311), and (222) crystal planes of face-centered cubic (fcc) Ag. The peaks at $2\theta = 44.8°$ and 76.8° correspond to the (111) and (220) planes of the fcc Ni, which overlap with the peaks of Ag and could not be observed. The peak at $2\theta = 52.2°$, corresponding to the (200) plane of the fcc Ni, reveals the existence of Ni in the composites. From the XRD results, as the mole ratios of [Ag]:[Ni] in the sources increased from [Ag]:[Ni] = 0.5:1 to [Ag]:[Ni] = 3:1, the peaks intensities of Ni at $2\theta = 44.8°$, 52.2°, and 76.8° of the three samples gradually decreased, indicating the increase of [Ag]:[Ni] in these three samples. XRF analysis was used to evaluate the real [Ag]:[Ni] ratios in three different samples with a designed [Ag]:[Ni] ratio of 0.5:1, 1:1 and 3:1, as shown in table 1. To get more reliable results, three different micro regions were analyzed in each sample and the average mole ratios were obtained. The measured [Ag]:[Ni] value in the sample with [Ag]:[Ni] = 0.5:1 is 0.49:1, which is consistent with the theoretical value. The measured mole ratios in samples with [Ag]:[Ni] = 1:1 and 3:1 are 1.12:1 and 3.58:1, respectively. The mole ratios are a little higher than the theoretical values due to the transmetallation reaction between Ag and Ni, in which a certain amount of Ni atoms were consumed and replaced by Ag^+, resulting in the decreased ratio of Ni.

According to the formation mechanism above, the morphologies of Ni@Ag NWs could be tailored from Ni wire-Ag particles to Ni core-Ag shell NWs by controlling the [Ag]:[Ni] and the morphologies of Ni@Ag NWs with different [Ag]:[Ni] are shown in figure 3.

The bare NiNWs display an average diameter of about 200 nm and an aspect ratio of 300, as shown in figures 3(a) and (b), which benefit the catalytic properties. When the [Ag]:[Ni] was 0.5:1, only a few Ag islands were formed on the surface of the NiNWs, exhibiting a wire-particle morphology as shown in figures 3(c) and (d). Thirty individual NWs were statistically analyzed to obtain the average diameter of 210 nm since some Ag^+ replaced Ni in the transmetallation process and a thin Ag shell was formed on the surface, increasing the diameter of the wires a little. From figures 3(e) and (f), as the [Ag]:[Ni] increased to 1:1, more sufficient Ag^+ were reduced to Ag islands and formed a thicker shell on the surface of the NiNW core with an average diameter of 370 nm. When the [Ag]:[Ni] increased to 3:1, more and more AgNPs were deposited and the surface of the wires were more uniform, leading to an even larger diameter of 410 nm. Besides, from figures 3(g) and (h), obvious aggregation of abundant AgNPs could be observed because of the excess $AgNO_3$.

Figure 4(a) shows a TEM image of the Ni@Ag NWs with [Ag]:[Ni] = 0.5:1. Several Ag particles were deposited on the surface of the wire. The HRTEM image of Ag shell presents the 0.23 and 0.21 nm lattice fringes, corresponding to the (111) and (200) planes of the fcc Ag respectively, as shown in figure 4(b). The SAED patterns of the Ni@Ag NWs are shown in figure 4(c), confirming the existence of Ag as well as Ni. TEM mapping was further conducted to study the elemental distributions of Ni and Ag in Ni@Ag NWs. As displayed in figures 4(d)–(f), a Ag nanoshell existed on the surface of the NiNW core, and some Ag islands were deposited on the core. The elemental mapping results proved that Ag fully covered the surface of the Ni core.

To further confirm that the Ni cores were fully covered by Ag nanoshells, the XPS spectra of Ni@Ag NWs with [Ag]:[Ni] = 1:1 in the Ni2p and Ag3d regions were measured. As shown in

figure 5(a), two binding energies of Ag3d at 367.8 and 373.8 eV could be observed clearly [37]. The Ni2p spectra could be decomposed into five peaks. The peak at 852.3 eV corresponds to metallic Ni^0 and the peaks at 855.4, 861.2, 873.1, and 878.8 eV are ascribed to Ni^{2+} in $Ni(OH)_2$ [38–40]. $Ni(OH)_2$ is formed owing to the existence of Ni^{2+} during the transmetallation reaction and the alkalinity of hydrazine hydrate, thus generating the complex of N_2H_4 and Ni^{2+} ions. The peak of Ni^0 almost disappeared in the Ni2p region, revealing that the NiNWs cores were almost covered by Ag nanoshells and the core shell structure of Ni@Ag NWs formed. The XPS results confirmed the formation of Ni@Ag core shell NWs and verified the synthesis mechanism illustrated in figure 1.

One of the aims in synthesizing the Ni@Ag core shell NWs is preventing the oxidation of NiNWs by coating with a Ag shell. The core shell morphologies are displayed in the SEM and TEM images above, but the effect of protection by Ag shells needs to be verified, which will affect the recyclability by magnetic field. TGA was used to investigate the anti-oxidation properties of Ni@Ag NWs. Ni was oxidized in air atmosphere, leading to the weight increase. However, the anti-oxidation property was improved and the weight increase was be much lower with the presence of a Ag shell. Pure NiNWs, Ni@Ag NWs with [Ag]:[Ni] = 1:1 and [Ag]:[Ni] = 0.5:1 were tested by TGA under air atmosphere and the results are shown in figure 6(a).

Figure 6(a) exhibits a slight weight loss of 1–5 wt% below 280 °C due to the loss of residual solvent for all three samples. Above 280 °C, as shown in the TGA curve of the pure NiNWs, the weight increased significantly for temperatures ranging from 300 °C–450 °C due to the oxidation of the NiNWs, then the weight further increased and gradually approached a stable value at 119% after 500 °C. The weight increment of 24% was near to the theoretical increment of 27%

for complete oxidation of Ni, as shown in figure 6(b). The TGA curve for Ni@Ag NWs with [Ag]:[Ni] = 0.5:1 also showed a gradual increase to 110% over the temperature range from 280°C–500 °C, which could be ascribed to the anti-oxidation by the AgNPs deposited on the surface of the NiNWs. The actual weight increment was 12%, which was lower than 17% of complete oxidation. For the Ni@Ag NWs with [Ag]:[Ni] = 1:1, only a weight increment of 5% was observed after 500 °C, much lower than 14% of complete oxidation, so the oxidation of the Ni cores was significantly prevented, revealing the largely improved anti-oxidation properties of Ni@Ag NWs compared to NiNWs.

Catalytic reduction of 4-NP

The reduction of 4-NP by $NaBH_4$ in water catalyzed by Ni@Ag NWs was monitored by a time-dependent UV–vis absorption spectra in the range of 250–500 nm. As shown in figure 7, the yellow solution of 4-NP and $NaBH_4$ could generate 4-NP ions, which shows a strong adsorption peak at 400 nm. With the addition of Ni@Ag NWs catalyst, the color of the solution gradually disappeared as the reaction proceeded. It can be observed in figure 7 that the adsorption peaks of 4-NP ions decreased with time and the peak of the product of 4-AP at 303 nm increased, indicating the catalytic reduction of 4-NP to 4-AP.

The Ni@Ag NWs possess an aspect ratio as high as 300, depending on the length of the NiNW core. The large aspect ratio results in a high surface area to volume (SA/V) ratio, which is the amount of surface area per unit volume of an object. The high SA/V ratio of the Ni@Ag NWs ensures a high catalyst surface exposed to reactants, leading to a high catalytic efficiency [20]. Hence, the Ni@Ag core shell NWs display fast and efficient catalytic reduction of 4-NP with a high SA/V ratio of 22.472 for the unit volume, compared to the sphere with the smallest SA/V ratio of 4.836 for the unit volume.

Figure 8 displays the plots of ln (c_t/c_0) versus reaction time for the reduction of 4-NP, where c_0 denotes the initial absorbance of 4-NP and c_t is the absorbance at a certain time. As shown in figure 8(a), the concentration of 4-NP decreased rapidly by the catalytic reduction of Ni@Ag NWs catalyst. As described above, Ni@Ag NWs with [Ag]:[Ni] = 1:1 possessed a thicker Ag shell, thus the amount of Ag was higher than the one with [Ag]:[Ni] = 0.5:1, leading to a higher catalytic activity. The concentrations of 4-NP decreased rapidly with the addition of Ni@Ag NWs and the whole catalytic reduction of 4-NP was completed in 8 min. Figure 8(b) shows kinetic plots of the catalytic reaction over Ni@Ag NWs. The reduction follows a pseudo-first-order kinetics with respect to 4-NP due to the presence of excessive $NaBH_4$. The reaction rate constant (k) is determined by the slope of a linear ln (c_t/c_0) verses t plot. As shown in the inset of figure 8(b), the Ni@Ag NWs catalyst with [Ag]:[Ni] = 1:1 shows a k of 0.408 s^{-1}, which is around 2 times higher than that of (0.257 s^{-1}) of [Ag]:[Ni] = 0.5:1. Since k is related to the weight of the catalysts, K' is defined as k over the weight of catalysts to estimate the performance of the catalysts. K' of Ni@Ag NWs catalyst with [Ag]:[Ni] = 0.5:1 and [Ag]:[Ni] = 1:1 were 51.3 and 81.5 $s^{-1}g^{-1}$, respectively.

3.3. Catalytic mechanism of Ni@Ag NWs catalyst

4-NP reduction by $NaBH_4$ is a 'model catalytic reaction' [41, 42]. The mechanism is proposed to illustrate the catalytic activity of the Ni@Ag NWs catalyst and a schematic diagram is shown in figure 9. Firstly, Ag shells capture the electrons from the BH_4^- ions, making the catalyst electrophilic. The solution becomes slightly alkaline by the BH_4^- generated from $NaBH_4$ and 4-NP ions could be obtained by ionization of 4-NP in a weak alkaline environment. Hence, 4-NP ions and BH_4^- are negatively charged and absorbed on the surface of Ni@Ag NWs catalyst according to the Langmuir–Hinshelwood mechanism [43, 44]. The $B(OH)_4^-$ and active hydrogen

are formed owing to the hydrolysis of $NaBH_4$ and the active hydrogen is transferred to the surface of the catalyst. Finally, the H at the surface of the Ag shell reacts with 4-NP, making 4-NP transform to 4-AP [45]. In summary, the reduction reaction could be expressed by equation (2) [9, 10, 44].

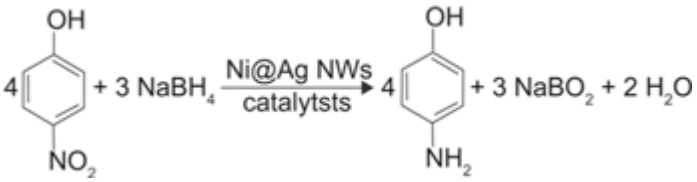

Magnetic recycle performance

Figure 10 shows the magnetic hysteresis loop of the sample with [Ag]:[Ni] = 0.5:1, 1:1, and 3:1 at room temperature. The saturation magnetization (Ms) of the three catalysts was measured to be 12.5, 10.8, and 7.7 emu g^{-1}, respectively. The Ms of these three samples decreased gradually as the amount of Ag increased, which could be mainly attributed to the decrease of the amount of Ni in the samples. However, the Ms is still large enough for magnetic separation of the catalyst from the solution with a magnet, as shown in the inset of figure 7, leading to high recyclability after repeated use.

The recyclability of Ni@Ag NWs catalyst was investigated with ten consecutive cycles. Figure 11 displays a histogram of the degradation and the plot of the rate constant k versus different cycles. It shows that the resultant catalyst can be recycled 10 times without obvious loss of the catalytic activity. Only 2.2% performance degraded after ten cycles and the k value in the tenth run is about 0.379 s^{-1}, 90% of that in the first run of 0.421 s^{-1}. This excellent recycling performance was due to the special core shell NW structure of the catalyst. The small size and weak magnetic interactions of the ordinary NP catalysts make them difficult to collect by an

external magnet. Some catalysts were lost while recycling and the cycle performance of the NP catalysts was not very satisfactory.

However, as the aspect ratio of the Ni nanostructures increases, the saturation magnetization Ms increases and the coercivity Hc decreases. The high aspect ratio of the NiNWs contributes to a high Ms and low Hc and vice versa [46, 47]. Hence, the NWs are more sensitive to the applied field than the particles with a lower aspect ratio. The Ni@Ag NWs catalyst is easy to collect by an external magnet, leading to excellent cycle performance with only 2.2% performance loss after ten cycles. Table 2 compares different kinds of catalysts reported in recent years and their catalytic performance as well as the recyclability. As shown in the table, the Ni@Ag NWs catalyst in this work shows high catalytic activity, excellent cycle performance, and long-term stability, and high potential in actual applications.

Conclusion

In summary, a new kind of morphology controllable Ni@Ag core shell NWs was proposed by a simple chemical reduction method with NiNWs as the precursor. A transmetallation reaction between Ni and Ag^{+} occurred, followed by the *in situ* reduction of Ag islands and the formation of a Ag shell in the layer-plus-island growth mode. The prepared Ni@Ag NWs were used as a catalyst for the reduction of 4-NP by $NaBH_4$ at room temperature and showed high catalytic activity over 4-NP with a rate constant of 0.408 s^{-1}. Moreover, the catalyst exhibited excellent cycle performance and can be recycled 10 times without an obvious loss of activity.

Acknowledgments

This work was supported by the National Natural Science Foundation of China (Grant Numbers 51702285, 51772269, 91748209, 11525210, and 11621062), and the Zhejiang Provincial Natural

Science Foundation (Grant Number LY17F040003). The authors also want to thank the support of the Open Projects Foundation of Yangtze Optical Fiber and the Cable Joint Stock Limited Company (YOFC) (Grant Number SKLD1708), 2017-HT-ZD, HKSAR (PolyU 153027/17P), and PolyU (G-SB82, 1-YBPU).

Author contributions

All authors have given approval to the final version of the manuscript.

Notes

There are no conflicts of interest to declare.

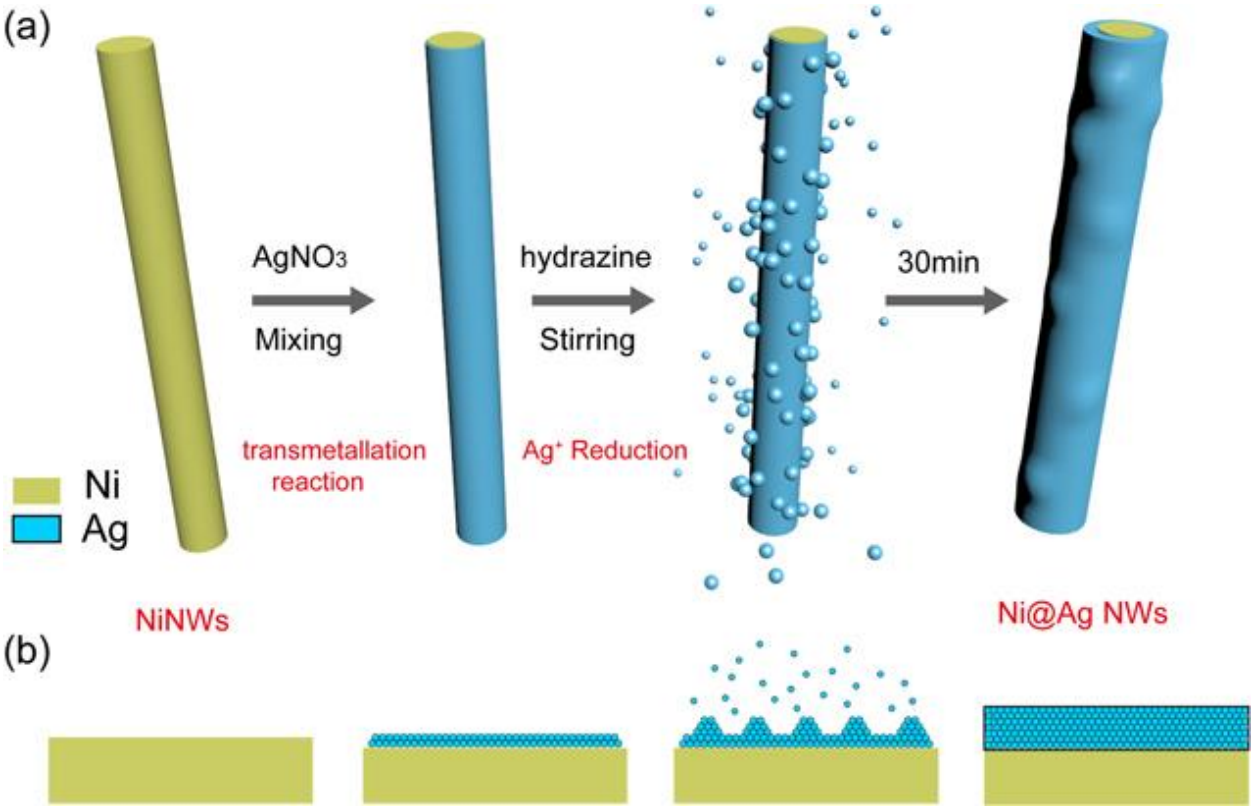

Figure 1. Schematic diagram of the synthesis of Ni@Ag core shell NWs.

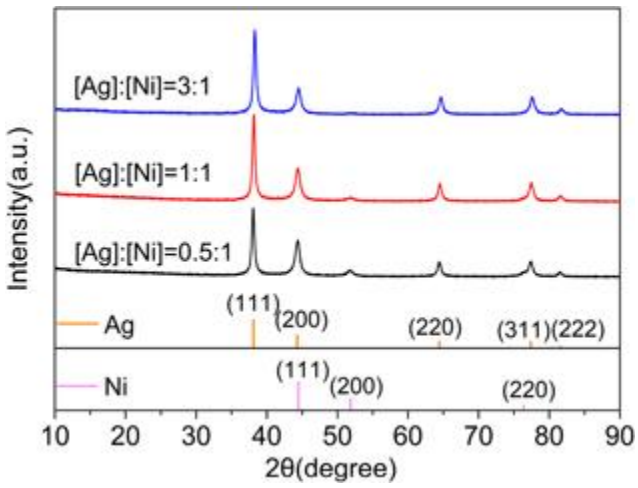

Figure 2. XRD patterns of the Ni@Ag NWs with different [Ag]:[Ni].

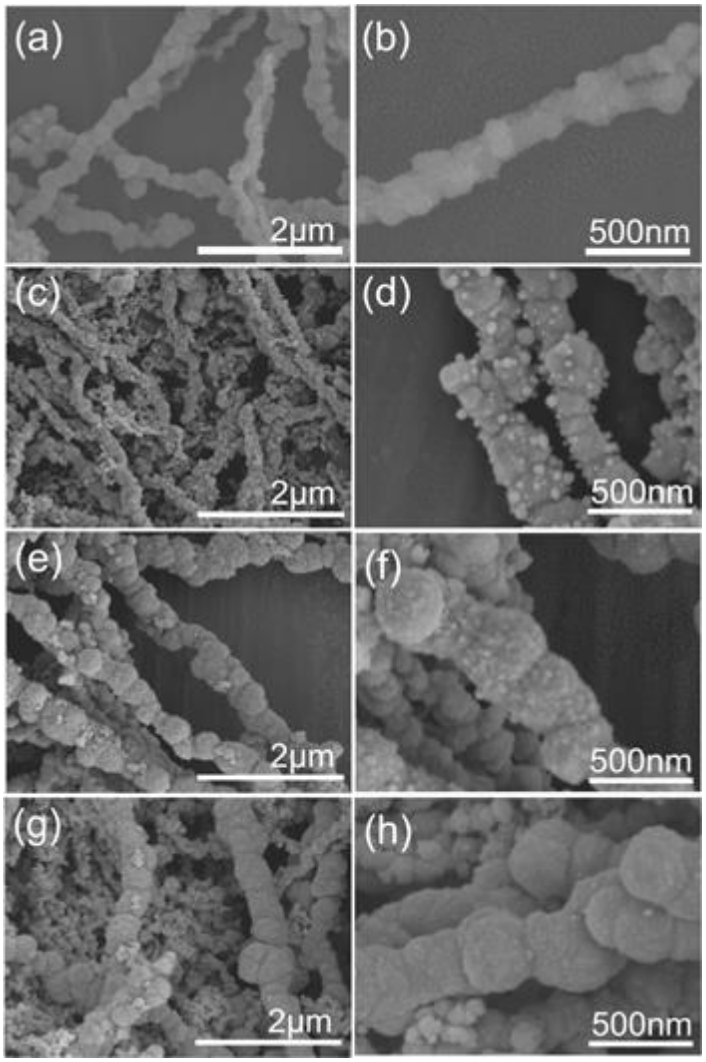

Figure 3. SEM images of Ni@Ag NWs with different mole ratios. (a), (b) Bare NiNWs; (c), (d) [Ag]:[Ni] = 0.5:1; (e), (f) [Ag]:[Ni] = 1:1; (g), (h) [Ag]:[Ni] = 3:1.

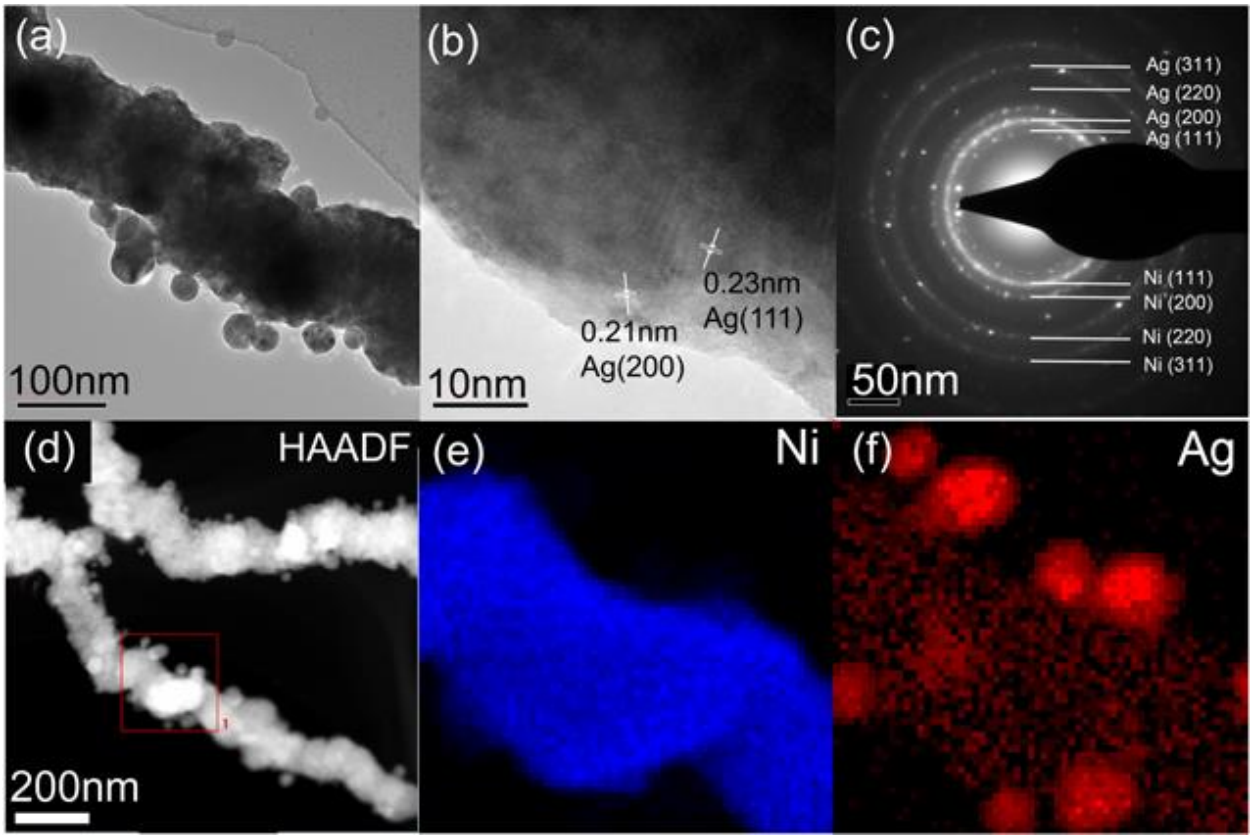

Figure 4. TEM image of (a) Ni@Ag NWs with [Ag]:[Ni] = 0.5:1 and (b) HRTEM image of the shell in an individual NW. (c) SAED patterns of the Ni@Ag NWs. (d)–(f) Energy dispersive spectrometer mapping analysis of the Ni@Ag NWs.

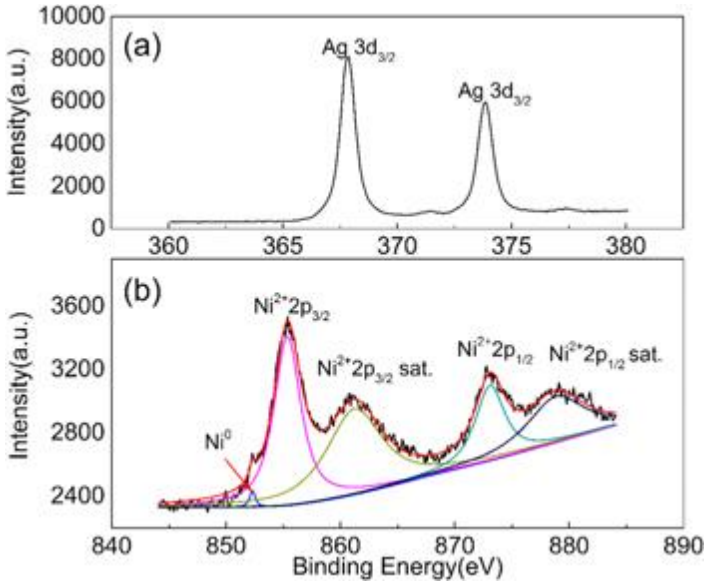

Figure 5. XPS spectra of Ni@Ag NWs with [Ag]:[Ni] = 1:1 in the (a) Ag3d and (b) Ni2p regions.

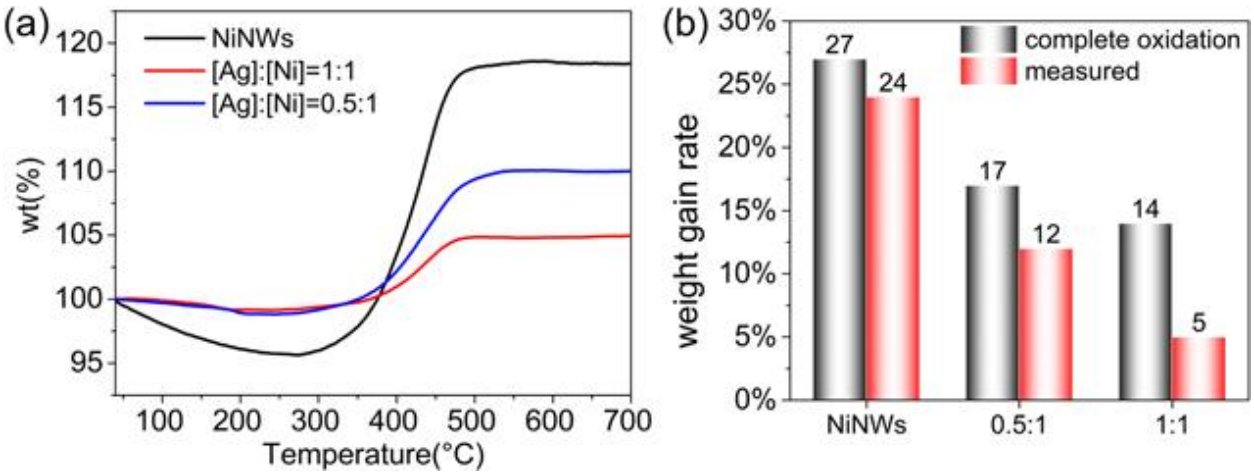

Figure 6. (a) TGA results under air atmosphere and (b) histogram of theoretical and measured weight increments of pure NiNWs, Ni@Ag NWs with [Ag]:[Ni] = 1:1 and [Ag]:[Ni] = 0.5:1.

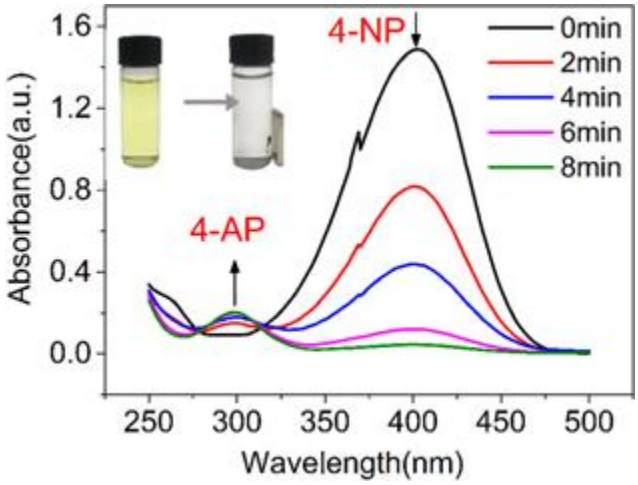

Figure 7. Time-dependent UV–vis absorption spectra for the reduction of 4-NP over the Ni@Ag NWs catalyst. The inset shows a photograph of the reduction and magnetic separation of the catalyst.

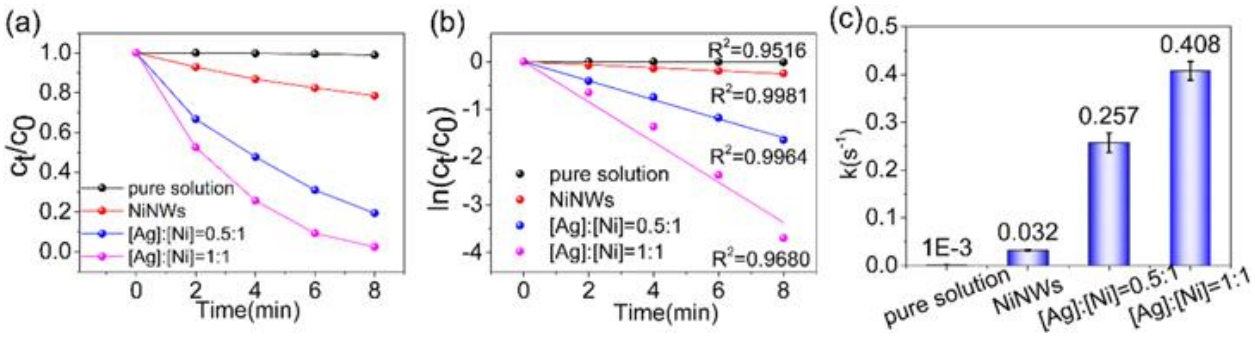

Figure 8. (a) Time-dependent concentrations (c_t/c_0) of 4-NP ions in the solution. (b) Plots of ln (c_t/c_0) versus reaction time for the reduction of 4-NP. (c) The corresponding kinetic constant k for the reduction of 4-NP over the pure solution, bare NiNWs, and Ni@Ag NWs catalyst with [Ag]:[Ni] = 0.5:1 and 1:1.

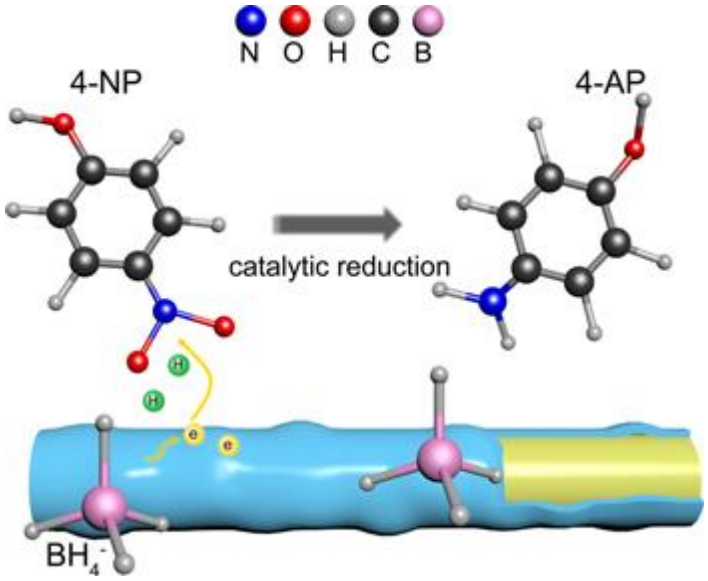

Figure 9. Schematic diagram of the catalytic mechanism of the Ni@Ag NWs catalyst.

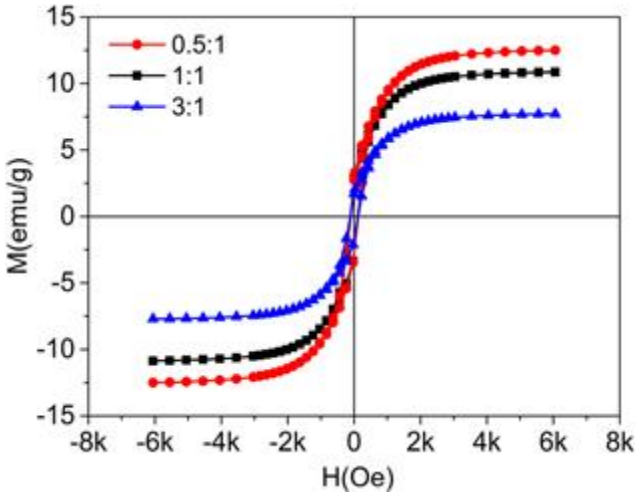

Figure 10. Magnetic hysteresis loops of Ni@Ag NWs catalyst.

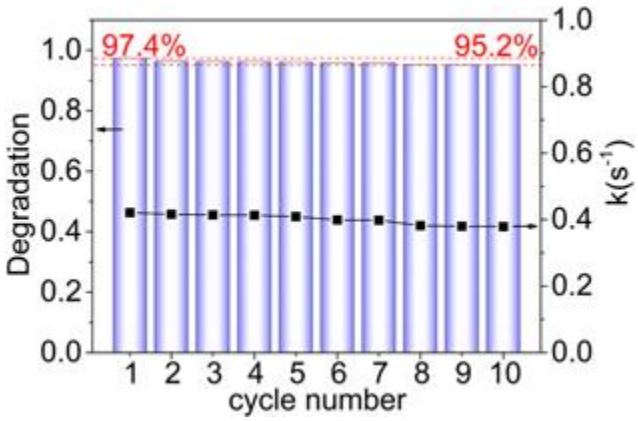

Figure 11. Performance degradation and the rate constant k of Ni@Ag NWs catalyst for the reduction of 4-NP with 10 times of cycling uses.

Table 1. XRF results of the samples with different designed mole ratios of [Ag]:[Ni] in the sources.

	[Ag]:[Ni] in sources		
Measured value	**0.5:1**	**1:1**	**3:1**
AgL (at%)	32.97	52.93	78.18
NiK (at%)	67.03	47.07	21.83
Average [Ag]:[Ni]	0.49:1	1.12:1	3.58:1

Table 2. Comparison of different catalysts and their performance.

Different catalysts	**k(s^{-1})**	**K'($s^{-1}g^{-1}$)**	**Cycle**	**Performance loss (%)**	**References**
Ni@PdNPs /KCC-1	0.020	51	6	5	[15]
AgNPs/HNTs	0.001	2	—	—	[23]
AuNPs/SNTs	0.011	1.325	—	—	[48]
Au/Fe NPs	0.313	57.96	11	2.94	[49]
Ni-Pd/NrGO	0.017	3400	10	10	[4]
Fe_3O_4@SiO_2@PEI-Au/Ag@PDA	0.009	93	8	4	[28]
Ni@Ag NWs	0.408	81.5	10	2.2	This work

Reference

[1] Atarod M, Nasrollahzadeh M and Sajadi S M 2016 Green synthesis of Pd/RGO/Fe3O4 nanocomposite using Withania coagulans leaf extract and its application as magnetically separable and reusable catalyst for the reduction of 4-nitrophenol J. Colloid Interf. Sci. 465 249–58

[2] Bhushan B, Chauhan A, Samanta S K and Jain R K 2000 Kinetics of biodegradation of p-nitrophenol by different bacteria Biochem. Biophys. Res. Commun. 274 626–30

[3] Dieckmann M S and Gray K A 1996 A comparison of the degradation of 4-nitrophenol via direct and sensitized photocatalysis in TiO2 slurries Water Res. 30 1169–83

[4] Feng J, Su L, Ma Y, Ren C, Guo Q and Chen X 2013 CuFe2O4 magnetic nanoparticles: A simple and efficient catalyst for the reduction of nitrophenol Chem. Eng. J. 221 16–24

[5] Higson F K 1992 Microbial degradation of nitroaromatic compounds Adv. Appl. Microbiol. 37 1–19

[6] Jiang Z, Jiang Q, Huang R, Sun M, Wang K, Kuang Q, Zhu Z Z and Xie Z 2018 Chemically initiated liquid-like behavior and fabrication of periodic wavy Cu/CuAu nanocables with enhanced catalytic properties Nanoscale 10 9012–20

[7] Lai B, Chen Z, Zhou Y, Yang P, Wang J and Chen Z 2013 Removal of high concentration p -nitrophenol in aqueous solution by zero valent iron with ultrasonic irradiation (US– ZVI) J. Hazard. Mater. 250–251 220–8

[8] Ruan M, Song P, Liu J, Li E and Xu W 2017 Highly efficient regeneration of deactivated Au/C catalyst for 4-nitrophenol reduction J. Phys. Chem. C 121 25882–9

[9] Yang K, Yan Y, Wang H, Sun Z, Chen W, Kang H, Han Y, Zhang W, Sun X and Li Z-X 2018 Monodisperse Cu/Cu2O@C core-shell nanocomposite supported on rGO layers as an efficient catalyst derived from Cu-based MOFs/ GO structure Nanoscale 10 17647–55

[10] Zhang W, Xiao X, An T, Song Z, Fu J, Sheng G and Cui M 2003 Kinetics, degradation pathway and reaction mechanism of advanced oxidation of 4-nitrophenol in water by a UV/H2O2 process J. Chem. Technol. Biotechnol. 78 788–94

[11] Gao S, Zhang Z, Liu K and Dong B 2016 Direct evidence of plasmonic enhancement on catalytic reduction of 4-nitrophenol over silver nanoparticles supported on flexible fibrous networks Appl. Catal. B 188 245–52

[12] Rode C V, Vaidya M J, Jaganathan R and Chaudhari R V 2001 Hydrogenation of nitrobenzene to p -aminophenol in a fourphase reactor: reaction kinetics and mass transfer effects Chem. Eng. Sci. 56 1299–304

[13] Vaidya M J, And S M K and Chaudhari R V 2003 Synthesis of p-aminophenol by catalytic hydrogenation of p-nitrophenol Org. Process Res. Dev. 7 202–8

[14] Kundu S, Mandal M, Ghosh S K and Pal T 2004 Photochemical deposition of SERS active silver nanoparticles on silica gel and their application as catalysts for the reduction of aromatic nitro compounds J. Colloid Interface Sci. 272 134–44

[15] Dong Z, Le X, Dong C, Zhang W, Li X and Ma J 2015 Ni@Pd core-shell nanoparticles modified fibrous silica nanospheres as highly efficient and recoverable catalyst for reduction of 4-nitrophenol and hydrodechlorination of 4-chlorophenol Appl. Catal. B 162 372–80

[16] Li J, Liu C Y and Liu Y 2012 Au/graphene hydrogel: Synthesis, characterization and its use for catalytic reduction of 4-nitrophenol J. Mater. Chem. 22 8426–30

[17] Gawande M B, Guo H, Rathi A K, Branco P S, Chen Y, Varma R S and Peng D-L 2013 First application of coreshell Ag@Ni magnetic nanocatalyst for transfer hydrogenation reactions of aromatic nitro and carbonyl compounds RSC Adv. 3 1050–4

[18] Hu C, Lan Y, Qu J, Hu X and Wang A 2006 Ag/AgBr/TiO2 visible light photocatalyst for destruction of azodyes and bacteria J. Phys. Chem. B 110 4066–72

[19] Jana S, Ghosh S K, Nath S, Pande S, Praharaj S, Panigrahi S, Basu S, Endo T and Pal T 2006 Synthesis of silver nanoshell-coated cationic polystyrene beads: a solid phase catalyst for the reduction of 4-nitrophenol Appl. Catal. A 313 41–9

[20] Miguel N D, Manzanedo J and Arias P L 2012 Testing of a Ni-Al2O3 catalyst for methane steam reforming using different reaction systems Chem. Eng. Technol. 35 720–8

[21] Pradhan N, Pal A and Pal T 2001 Catalytic reduction of aromatic nitro compounds by coinage metal nanoparticles Langmuir 17 1800–2

[22] Liang M, Wang L, Su R, Qi W, Wang M, Yu Y and He Z 2013 Synthesis of silver nanoparticles within cross-linked lysozyme crystals as recyclable catalysts for 4-nitrophenol reduction Catal. Sci. Technol. 3 1910–4

[23] Liu P and Zhao M 2009 Silver nanoparticle supported on halloysite nanotubes catalyzed reduction of 4-nitrophenol (4-NP) Appl. Surf. Sci. 255 3989–93

[24] Chen D-H and Wang S-R 2006 Protective agent-free synthesis of Ni–Ag core-shell nanoparticles Mater. Chem. Phys. 100 468–71 [25] Gupta V K, Yola M L, Eren T, Kartal F, Çağlayan M O and Atar N 2014 Catalytic activity of Fe@Ag nanoparticle involved calcium alginate beads for the reduction of nitrophenols J. Mol. Liq. 190 133–41

[26] Lee C-C and Chen D-H 2006 Large-scale synthesis of Ni-Ag core-shell nanoparticles with magnetic, optical and antioxidation properties Nanotechnology 17 3094–103

[27] Singh S and Bahadur D 2015 Catalytic and antibacterial activity of Ag decorated magnetic core shell nanosphere Colloid. Surf. C 133 58–65

[28] Yu X, Cheng G and Zheng S Y 2016 Synthesis of selfassembled multifunctional nanocomposite catalysts with highly stabilized reactivity and magnetic recyclability Sci. Rep. 6 25459

[29] Zhu M, Wang C, Meng D and Diao G 2013 In situ synthesis of silver nanostructures on magnetic Fe3O4@C core–shell nanocomposites and their application in catalytic reduction reactions J. Mater. Chem. A 1 2118–25

[30] Roy A, Srinivas V, Ram S and Rao T V C 2007 The effect of silver coating on magnetic properties of oxygen-stabilized tetragonal Ni nanoparticles prepared by chemical reduction J. Phys.: Condens. Matter 19 6200–16

[31] Cañamares M V, Garcia-Ramos J V, Gómez-Varga J D, Domingo C and Sanchez-Cortes S 2005 Comparative study of the morphology, aggregation, adherence to glass, and surface-enhanced Raman scattering activity of silver nanoparticles prepared by chemical reduction of Ag+ using citrate and hydroxylamine Langmuir 21 8546–53

[32] Hu H, Xin J H, Hu H, Wang X, Miao D and Liu Y 2015 Synthesis and stabilization of metal nanocatalysts for reduction reactions-a review J. Mater. Chem. A 3 11157–82

[33] Deshmukh S P, Dhokale R K, Yadav H M, Achary S N and Delekar S D 2013 Titania–supported silver nanoparticles: an efficient and reusable catalyst for reduction of 4-nitrophenol Appl. Surf. Sci. 273 676–83

[34] Wang S, Chen K F, Wang M, Li H S, Chen G R, Liu J, Xu L H, Jian Y, Meng C D and Zheng X Y 2018 Controllable synthesis of nickel nanowires and the application in high sensitivity, stretchable strain sensor for body motion sensing J. Mater. Chem. C 6 4737–45

[35] Ruiz R, Choudhary D, Nickel B, Toccoli T, Chang K, Mayer A C, Clancy P, Blakely J M, Headrick R L, Iannotta S and Malliaras G G 2004 Pentacene thin film growth Chem. Mater. 16 4497–508

[36] Seo J, Kim T-H and Kuk Y 2015 Visualization of the inverse layer-plus-island growth in Fe islands on W(110) substrate Curr. Appl Phys. 15 1042–8

[37] Chook S W, Chia C H, Zakaria S, Ayob M K, Chee K L, Huang N M, Neoh H M, Lim H N, Jamal R and Rahman R 2012 Antibacterial performance of Ag nanoparticles and AgGO nanocomposites prepared via rapid microwaveassisted synthesis method Nanoscale Res. Lett. 7 541–2

[38] Han K, Kreuger T, Mei B and Mul G 2017 Transient behavior of Ni@NiOx functionalized SrTiO3 in overall water splitting ACS Catal. 7 1610–4

[39] Park K W, Choi J H, Kwon B K, Lee S A and Sung Y E 2002 Chemical and electronic effects of Ni in Pt/Ni and Pt/Ru/ Ni alloy nanoparticles in methanol electrooxidation J. Phys. Chem. B 106 1869–77 [

40] Shubin Y, Xilin W, Changlun C, Huanli D, Wenping H and Xiangke W 2012 Spherical α-Ni(OH)2 nanoarchitecture grown on graphene as advanced electrochemical pseudocapacitor materials Chem. Commun. 48 2773–8

[41] Wunder S, Lu Y, Albrecht M and Ballauff M 2011 Catalytic activity of faceted gold nanoparticles studied by a model reaction: evidence for substrate-induced surface restructuring ACS Catal. 1 908–16

[42] Xu W, Kong J S, Yeh Y T E and Chen P 2008 Single-molecule nanocatalysis reveals heterogeneous reaction pathways and catalytic dynamics Nat. Mater. 7 992–8

[43] Lin F-H and Doong R-A 2014 Highly efficient reduction of 4-nitrophenol by heterostructured gold-magnetite nanocatalysts Appl. Catal. A 486 32–41

[44] Liu L, Chen R, Liu W, Wu J and Gao D 2016 Catalytic reduction of 4-nitrophenol over Ni-Pd nanodimers supported on nitrogen-doped reduced graphene oxide J. Hazard. Mater. 320 96–104

[45] Aditya T, Pal A and Pal T 2015 Nitroarene reduction: a trusted model reaction to test nanoparticle catalysts Chem. Commun. 51 9410–31

[46] He X, Zhong W, Au C T and Du Y 2013 Size dependence of the magnetic properties of Ni nanoparticles prepared by thermal decomposition method Nanoscale Res. Lett. 8 446–56

[47] Singh A K, Srivastava O N and Singh K 2017 Shape and sizedependent magnetic properties of Fe3O4 nanoparticles synthesized using piperidine Nanoscale Res. Lett. 12 298–305
[48] Zhang Z, Shao C, Zou P, Zhang P, Zhang M, Mu J, Guo Z, Li X, Wang C and Liu Y 2011 In situ assembly of well-dispersed gold nanoparticles on electrospun silica nanotubes for catalytic reduction of 4-nitrophenol Chem. Commun. 47 3906–14
[49] Chang Y-C and Chen D-H 2009 Catalytic reduction of 4-nitrophenol by magnetically recoverable Au nanocatalyst J. Hazard. Mater. 165 664–73